metals

MDPI

Article

# Role of Severe Plastic Deformation in Suppressing Formation of R Phase and $Ni_4Ti_3$ Precipitate of NiTi Shape Memory Alloy

**Li Hu [1,2], Shuyong Jiang [1,*] and Yanqiu Zhang [1]**

[1] College of Mechanical and Electrical Engineering, Harbin Engineering University, Harbin 150001, China; heu_huli@126.com (L.H.); zhangyanqiu0924@sina.com (Y.Z.)
[2] College of Materials Science and Chemical Engineering, Harbin Engineering University, Harbin 150001, China
* Correspondence: jiangshuyong@hrbeu.edu.cn; Tel.: +86-451-8251-9710

Academic Editor: Takuo Sakon
Received: 22 March 2017; Accepted: 17 April 2017; Published: 19 April 2017

**Abstract:** Microstructural evolution of NiTi shape memory alloy (SMA) with a nominal composition of $Ni_{50.9}Ti_{49.1}$ (at %) is investigated on the basis of heat treatment and severe plastic deformation (SPD). As for as-rolled NiTi SMA samples subjected to aging, plenty of R phases appear in the austenite matrix. In terms of as-rolled NiTi SMA samples undergoing solution treatment and aging, $Ni_4Ti_3$ precipitates arise in the austenite matrix. In the case of as-rolled NiTi SMA samples subjected to SPD and aging, martensitic twins are observed in the matrix of NiTi SMA. With respect to as-rolled NiTi SMA samples subjected to solution treatment, SPD, and aging, neither R phases nor $Ni_4Ti_3$ precipitates are observed in the matrix of NiTi SMA. The dislocation networks play an important role in the formation of the R phase. SPD leads to amorphization of NiTi SMA, and in the case of annealing, amorphous NiTi SMA samples are subjected to crystallization. This contributes to suppressing the occurrence of R phase and $Ni_4Ti_3$ precipitate in NiTi SMA.

**Keywords:** shape memory alloy; NiTi alloy; severe plastic deformation; microstructure

## 1. Introduction

NiTi shape memory alloys (SMAs) have been widely used in aviation, medical, dental, and automotive fields because of their excellent abrasion resistance, good functional properties, and high mechanical properties [1,2]. Furthermore, plastic deformation and heat treatment have a significant influence on the microstructures of SMAs, which consequently affect their operation performance [3–5]. In general, solution treatment leads to one-step transformation of NiTi SMAs from austenite (B2 structure) to martensite (B19′ structure). Solution treatment along with aging results in the precipitation of $Ni_4Ti_3$ phase, which further contributes to the occurrence of two-stage transformation, three-stage transformation, or even four-stage transformation of NiTi SMAs [6–9]. It has been proposed that the existence of $Ni_4Ti_3$ precipitates contribute to the emergence of the R phase, which plays a significant role in multiple-stage transformation of SMAs. Severe plastic deformation (SPD) methods, such as high pressure torsion (HPT) [10,11], cold drawing [12,13], cold rolling [14], surface mechanical attrition treatment (SMAT) [15], and local canning compression [16], can lead to amorphization of NiTi SMAs at lower temperatures. In addition, amorphous NiTi SMA induced by means of SPD is able to be subjected to crystallization in the case of proper heat treatment, where even nanocrystalline NiTi SMA can be produced. However, almost no literature has reported the influence of SPD and subsequent heat treatment on the formation of $Ni_4Ti_3$ precipitates and the R phase.

Based on local canning compression, comprehensive influence of heat treatment, as well as SPD on microstructural evolution of NiTi SMA was investigated in the present work. The influence of SPD and subsequent heat treatment on the formation of $Ni_4Ti_3$ precipitate and R phase, in particular, have been emphasized.

## 2. Materials and Methods

A NiTi SMA bar, which possesses the nominal composition of $Ni_{50.9}Ti_{49.1}$ (at %), was manufactured by virtue of vacuum induction melting followed by hot rolling. In order to obtain the transformation temperatures of the NiTi SMA bar, differential scanning calorimetry (DSC) test was conducted on a DSC-204 type equipment (Netzsch Group, Freistaat Bayern, Germany). During the DSC test, both the heating rate and cooling rate were set as 10 °C/min and the temperatures ranged from −100 to 100 °C. Consequently, the transformation temperatures of NiTi SMA bar are determined as: $Ms$ = −27.2 °C, $Mf$ = −41.7 °C, $As$ = −17.3 °C, $Af$ = −4.1 °C. The as-rolled NiTi SMA bar was cut into halves, where one half was subjected to a solution treatment at 850 °C for 2 h and subsequently was quenched into ice water, and the other half was used for a contrast sample. Subsequently, the samples with the a diameter of 4 mm and the height of 6 mm were removed from the as-rolled and solution-treated NiTi SMA samples by virtue of electro-discharge machining (EDM) (DK7725, Jiangsu Dongqing CNC Machine Tool Co., Ltd., Taizhou, China), respectively. Afterward, these NiTi SMA samples were inserted into low carbon steel cans (Baosteel, Shanghai, China) which possess an inner diameter of 4 mm, outer diameter of 10 mm, and height of 3 mm. The locally canned NiTi SMA samples were compressed between the two anvils of the INSTRON 5500R equipment (Instron Corporation, Norwood, MA, USA) by 75% in height at the strain rate of 0.05 $s^{-1}$ and at room temperature, as shown in Figure 1. It can be noted that the NiTi SMA samples are under a three-dimensional compressive stress state due to the constraint of the steel cans. After the compression, the NiTi SMA samples were removed from the steel cans, respectively. Two samples with the diameter of 4 mm and the height of 6 mm were cut from the as-rolled NiTi SMA bar and the solution-treated NiTi SMA bar, respectively. Finally, the two samples along with a compressed sample were aged for 2 h at 600 °C and then they were cooled to room temperature in the ambient atmosphere. All the NiTi SMA samples that were subjected to heat treatment were vacuum-sealed in quartz tubes separately.

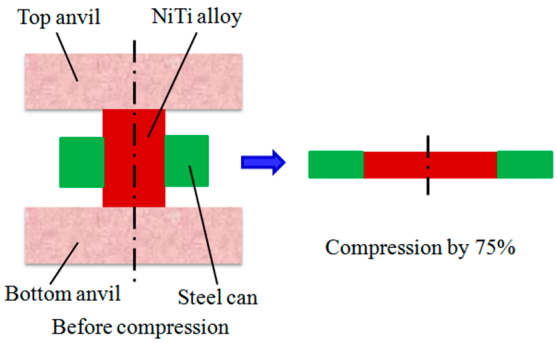


**Figure 1.** Schematic diagram of NiTi SMA sample subjected to local canning compression.

Microstructural evolution of the NiTi SMA samples was characterized using transmission electron microscopy (TEM). Foils used for TEM characterization were ground to 70 μm by virtue of mechanical method and subsequently were thinned by means of twin-jet polishing in an electrolyte with the composition of 6% $HClO_4$, 34% $C_4H_{10}O$ and 60% $CH_3OH$ (volume fraction). TEM observations were implemented on a FEI TECNAI G2 F30 type microscope (FEI Corporation, Hillsboro, OR, USA), which possesses a side-entry and double-tilt specimen stage with an angular range of ±40°.

## 3. Results

### *3.1. Microstructures of As-Rolled and Solution-Treated NiTi SMA Samples*

The microstructures of as-rolled NiTi SMA sample are shown in Figure 2. It can be found from Figure 2 that plenty of dislocations are distributed in the B2 austenite matrix. It can be deduced that plenty of dislocations are induced by plastic deformation. However, in the case of solution treatment, plenty of dislocations have disappeared in the B2 austenite matrix, as shown in Figure 3.

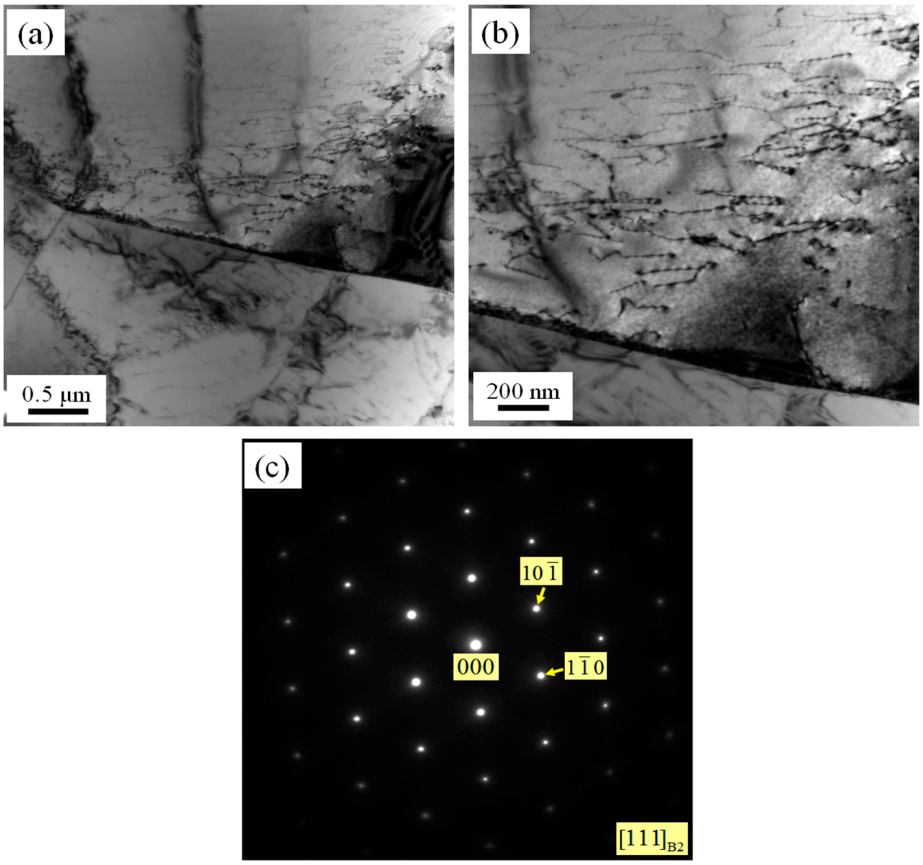


**Figure 2.** TEM micrographs of as-rolled NiTi SMA sample: (**a**) Bright field image (low magnification); (**b**) Bright field image (high magnification); (**c**) Diffraction pattern of (**b**).

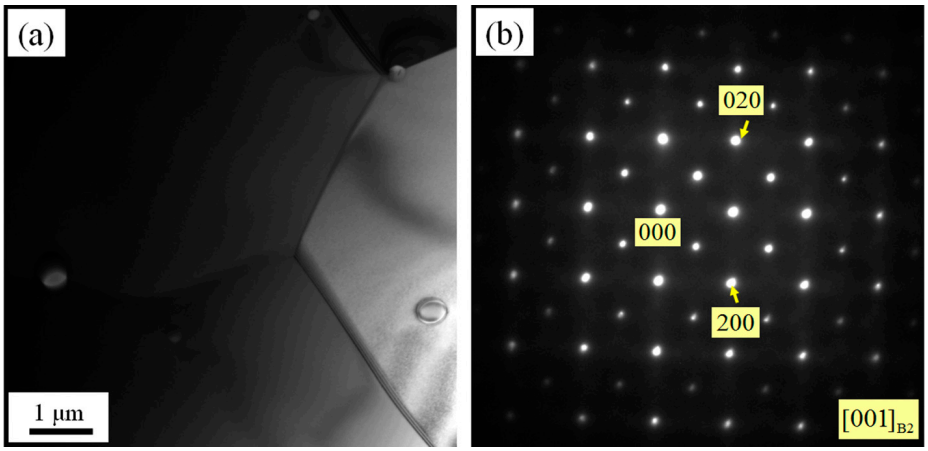


**Figure 3.** TEM micrographs of solution-treated NiTi SMA sample: (**a**) Bright field image; (**b**) Diffraction pattern of (**a**).

### *3.2. Microstructures of NiTi SMA Samples Subjected to SPD*

In the case of local canning compression, the as-rolled NiTi SMA sample is subjected to SPD so that a mixture of amorphous and nanocrystalline phases appears, where a small amount of nanocrystalline phase is distributed in the dominant amorphous matrix, as shown in Figure 4. In the same manner, solution-treated NiTi SMA samples exhibit a mixture of amorphous and nanocrystalline phases after suffering from SPD as well, but the amorphization seems to be completed more thoroughly, as shown in Figure 5.

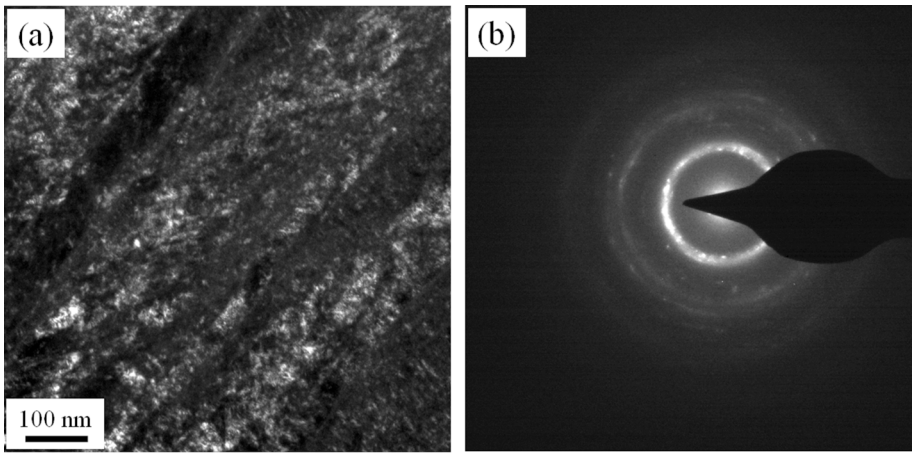


**Figure 4.** TEM micrographs of as-rolled NiTi SMA sample subjected to SPD: (**a**) Dark field image; (**b**) Diffraction pattern of (**a**).

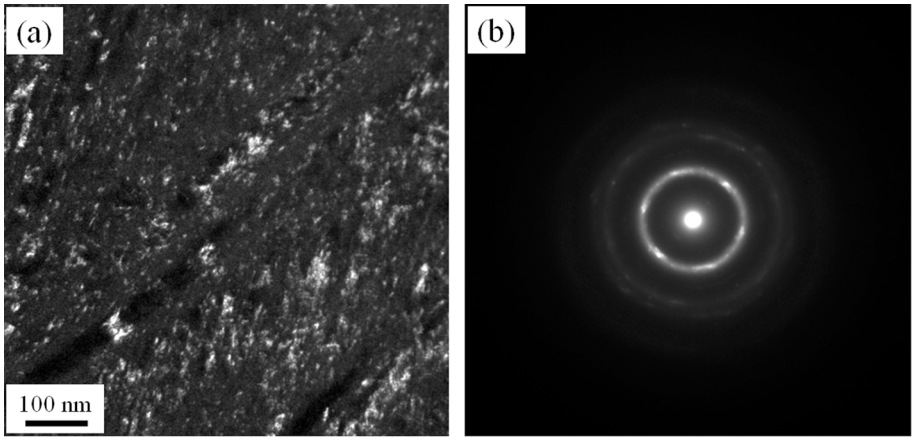


**Figure 5.** TEM micrographs of solution-treated NiTi SMA sample subjected to SPD: (**a**) Dark field image; (**b**) Diffraction pattern of (**a**).

### *3.3. Microstructures of As-Rolled NiTi SMA Sample Subjected to Aging*

Figure 6 shows TEM micrographs of as-rolled NiTi SMA sample subjected to aging. It can be observed from Figure 6 that R phase appears in the B2 austenite matrix of NiTi SMA. In addition, there is a certain orientation relationship between R phase and B2 austenite. It is generally accepted that the appearance of the R phase is attributed to the existence of $Ni_4Ti_3$ precipitate. However, it seems that no obvious diffraction pattern with respect to $Ni_4Ti_3$ precipitate is captured in the present work.

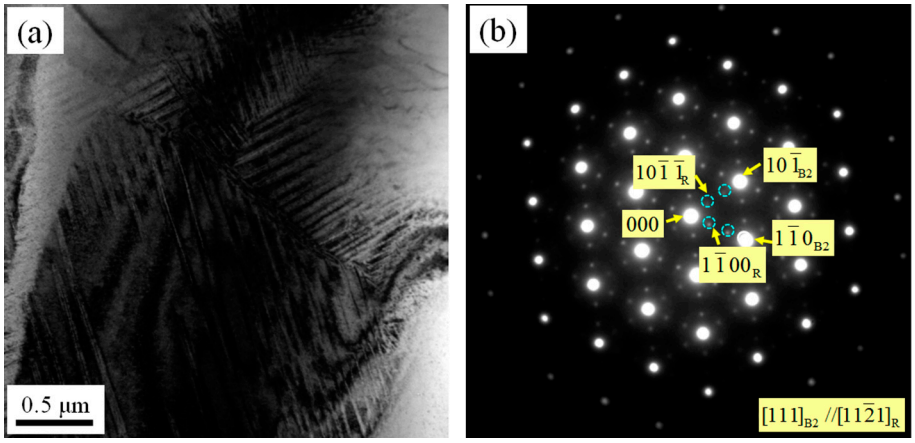


**Figure 6.** TEM micrographs of an as-rolled NiTi SMA sample subjected to aging: (**a**) Bright field image; (**b**) Diffraction pattern of (**a**).

### *3.4. Microstructures of NiTi SMA Sample Subjected to Solution Treatment and Aging*

Figure 7 shows TEM micrographs of NiTi SMA sample subjected to solution treatment and aging. It can be found from Figure 7 that the $Ni_4Ti_3$ precipitates exhibit the inhomogeneous distribution in the matrix of NiTi SMA sample and they are characterized by a typical lenticular shape [9]. In addition, it can be observed from Figure 6 that the $Ni_4Ti_3$ precipitates arise in the grain interior as well as in the grain boundary pinned by TiC phase and they are obviously coarser in the grain interior than in the grain boundary.

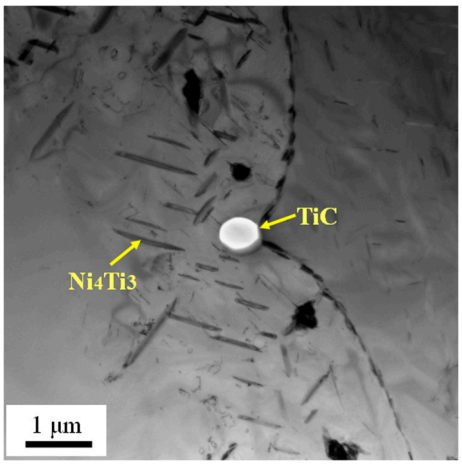


**Figure 7.** TEM micrographs of a solution-treated NiTi SMA sample subjected to aging.

### *3.5. Microstructures of As-Rolled NiTi SMA Sample Subjected to SPD and Aging*

Figure 8 shows the microstructures of an as-rolled NiTi SMA sample subjected to SPD and subsequent aging. It can be observed from Figure 8 that the microstructure of NiTi SMA sample has a feature of martensite morphology. Furthermore, it can be found that martensite twins are distributed in the matrix. The phenomenon has been validated by the previous study [17]. In addition, neither R phase nor $Ni_4Ti_3$ precipitate appear in the matrix of NiTi SMA.

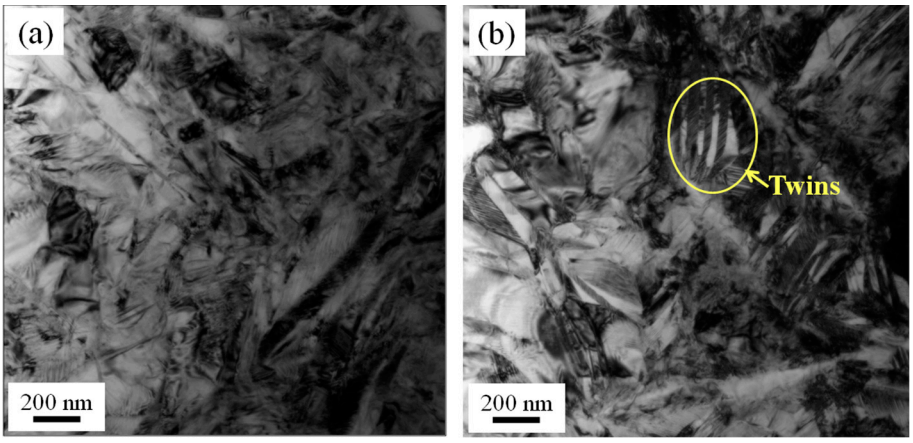


**Figure 8.** TEM micrographs of an as-rolled NiTi SMA sample subjected to SPD and subsequent aging: (**a**) Bright field image showing martensite morphology; (**b**) Bright field image showing the existence of martensite twins.

### *3.6. Microstructures of Solution-Treated NiTi SMA Sample Subjected to SPD and Aging*

Figure 9 TEM micrographs of solution-treated NiTi SMA sample subjected to SPD and subsequent aging. It can be found from Figure 9 that, as for solution-treated NiTi SMA samples subjected to SPD and subsequent aging, B2 austenite phase and B19′ martensite phase coexist in the matrix of NiTi SMA. In particular, neither R phase nor $Ni_4Ti_3$ precipitate appear in the matrix of NiTi SMA as well.

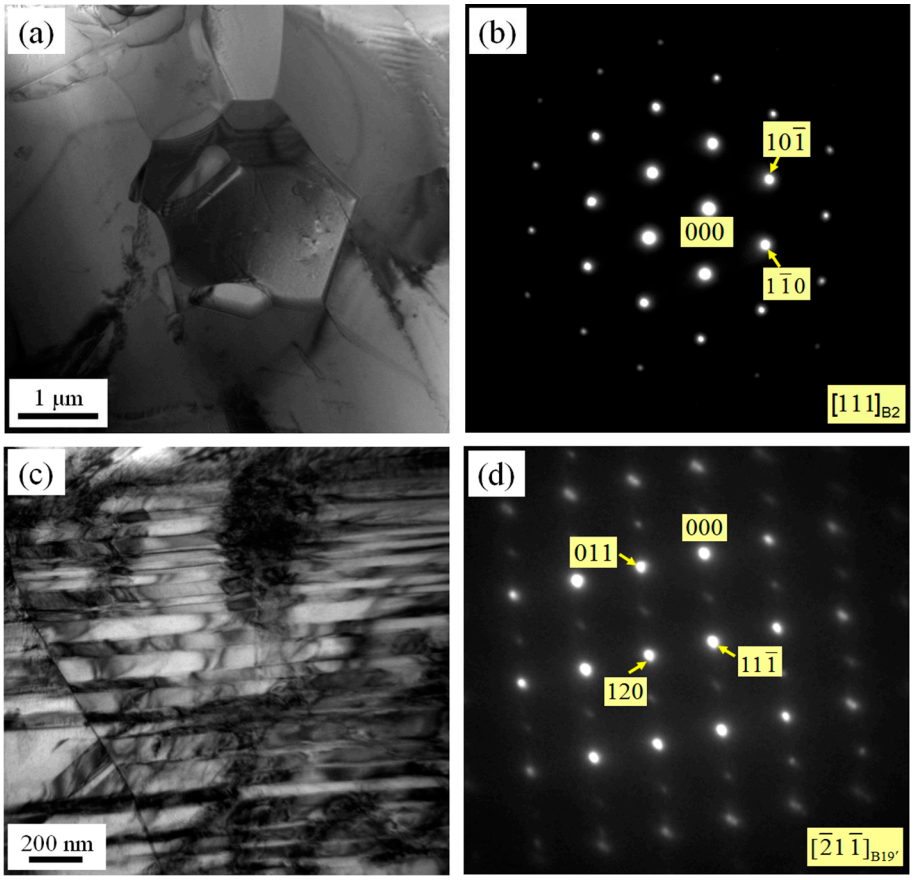


**Figure 9.** TEM micrographs of a solution-treated NiTi SMA sample subjected to SPD and subsequent aging: (**a**) Bright field image showing B2 austenite phase; (**b**) Diffraction pattern of (**a**); (**c**) Bright field image showing B19' martensite phase; (**d**) Diffraction pattern of (**c**).

## 4. Discussion

In general, $Ni_4Ti_3$ precipitates are nucleated and grow preferentially at the grain boundary on the basis of the theory for phase transformation kinetics. The nucleation rate of the $Ni_4Ti_3$ precipitates at the grain boundary is greater than that in the grain interior because nucleation barrier of the former is lower than that of the latter. Furthermore, the grain boundary energy plays an important role in accelerating the nucleation of $Ni_4Ti_3$ precipitates at the grain boundary. However, in the present study, the curvature of the grain boundary pinned occurs due to the pinning effect of the secondary phase TiC at the grain boundary. As a consequence, the grain boundary energy is reduced as compared to the original grain boundary, which suppresses the nucleation and growth of the $Ni_4Ti_3$ precipitates to a certain degree. However, whether the grain boundary is pinned or not, the nucleation rate of these $Ni_4Ti_3$ precipitates at the grain boundary is always greater than that in the grain interior. Firstly, the nucleation and growth of $Ni_4Ti_3$ precipitates at the grain boundary results in the Ni concentration at grain boundary being lowered as compared to the grain interior, which causes the Ni atoms in the interior of grain to diffuse towards the grain boundary. However, coherent interface is unable to be formed between the $Ni_4Ti_3$ precipitates at grain boundary and the B2 matrix, so the $Ni_4Ti_3$ phases at the grain boundary are hard to grow towards the grain interior due to the impediment of grain boundary. With the proceeding of aging, the $Ni_4Ti_3$ precipitates are nucleated and grow along the coherent interface between them and the B2 matrix in the grain interior. In addition, because the $Ni_4Ti_3$ phases in the grain interior can absorb Ni atoms from the B2 austenite matrix around them, they grow to be larger and larger, and consequently the smaller $Ni_4Ti_3$ precipitates are gradually merged by the larger $Ni_4Ti_3$ precipitates.

It is generally accepted that the existence of the $Ni_4Ti_3$ phases is able to suppress the transformation of martensite, which consequently promotes the occurrence of R phase. Because R phase plays an important role in multi-stage phase transformation of NiTi SMAs, the occurrence of two-stage phase transformation (B2-R-B19′) is regarded as a reasonable phenomenon in Ni-rich NiTi SMAs subjected to aging. However, abnormal three-stage transformation often appears in the aged Ni-rich NiTi SMAs. Bataillard et al. [18] suggested that the small-scale stress inhomogeneity in the B2 austenite matrix around $Ni_4Ti_3$ precipitates is responsible for the emergence of three-stage transformation during cooling, where the three-stage transformation includes an one-stage transformation from B2 austenite to R phase and a two-stage transformation from R phase to B19′ martensite, which corresponds to the high stress region near $Ni_4Ti_3$ precipitate and the low stress region away from $Ni_4Ti_3$ precipitate, respectively. Khalil Allafi et al. [19] suggested that the three-stage transformation during cooling is induced by the small-scale chemical composition inhomogeneity in the B2 austenite matrix and between the $Ni_4Ti_3$ precipitates, which leads to one B2-R transformation as well as two R-B19' transformations. Furthermore, the two R-B19' transformations occur in a low Ni region near $Ni_4Ti_3$ precipitate or at high Ni region away from $Ni_4Ti_3$ precipitate. Dlouhý et al. [20] gave microstructural evidence that R phase is nucleated at the interface between the B2 austenite matrix and $Ni_4Ti_3$ precipitate and B19′ martensite is nucleated at the interface between R phase and $Ni_4Ti_3$ precipitate. According to the aforementioned literatures, it can be proposed that the occurrence of R phase is mainly attributed to the inhomogeneous stress filed or the heterogeneous chemical composition, which results from the existence of $Ni_4Ti_3$ precipitates. However, in the present study, it seems that the dislocation networks lay the foundation for the formation of R phase. Under the condition of aging for 2 h at 600 °C, the $Ni_4Ti_3$ precipitates are easier to occur in the solution-treated NiTi SMA as compared to NiTi SMA which contains plenty of dislocations due to previous processing history.

When NiTi SMA is subjected to local canning compression, SPD results in amorphization of NiTi SMA. Crystallization of the amorphous NiTi SMA takes place in the course of subsequent aging for 2 h at 600 °C. As a matter of fact, SPD results in a mixture containing the amorphous phase and the retained nanocrystalline phase. The crystallization mechanism for the amorphous phase accompanied by the retained nanocrystalline phase can be summarized as the following procedures. Firstly, the retained nanocrystalline phase preferentially acts as the nucleus under the action of thermal driving force. In addition, a high density of dislocations is able to be induced in the retained

nanocrystalline phase, where the stored energy is enhanced. As a consequence, the release of the stored energy makes a contribution to the formation of the crystal nucleus. With the proceeding of aging time, new crystals are nucleated in the amorphous matrix because the stored energy aroused by the lattice defects of the amorphous phase is relaxed, and simultaneously the retained nanocrystals continue to grow up under the thermal driving force. Once all the grains impinge each other, complete crystallization occurs in the NiTi SMA sample suffering from SPD. Consequently, the amorphous phase is preferentially crystallized in the studied NiTi SMA, which contributes to suppressing the formation of $Ni_4Ti_3$ precipitates because the crystallized NiTi SMA is unable to meet the requirements for the precipitation of $Ni_4Ti_3$ phase. On the one hand, the energy has been consumed by the crystallization process and consequently the crystallized NiTi SMA is unable to meet the requirements for the precipitation of $Ni_4Ti_3$ phase in terms of energy. On the other hand, the crystallized NiTi SMA does not meet the requirements for the precipitation of $Ni_4Ti_3$ phase in terms of chemical composition. It can be concluded that SPD plays a significant role in suppressing the formation of R phase and $Ni_4Ti_3$ precipitate of NiTi SMA.

## 5. Conclusions

(1) In the case of as-rolled NiTi SMA sample subjected to aging for 2 h at 600 °C, R phase appears in the B2 austenite matrix. The as-rolled NiTi SMA sample contains plenty of dislocation networks aroused by previous processing history. The dislocation networks are responsible for the formation of the R phase.

(2) Solution treatment for 2 h at 850 °C can result in the annihilation of the dislocations in the as-rolled NiTi SMA sample. As a consequence, the $Ni_4Ti_3$ precipitates more easily arise in a solution-treated NiTi SMA sample when aged for 2 h at 600 °C.

(3) SPD is capable of inducing amorphization of a NiTi SMA sample at room temperature. Amorphous NiTi SMA is able to be subjected to crystallization when aged for 2 h at 600 °C. Consequently, SPD and subsequent aging contribute to enhancing the transformation temperature of martensite. In addition, SPD plays an important role in suppressing the occurrence of R phase and $Ni_4Ti_3$ precipitate.

**Acknowledgments:** The work was financially supported by National Natural Science Foundation of China (Nos. 51475101, 51305091 and 51305092).

**Author Contributions:** Li Hu performed the experiments and wrote the manuscript; Shuyong Jiang supervised the research; Yanqiu Zhang performed TEM analysis.

**Conflicts of Interest:** The authors declare no conflict of interest.

## References

1. Otsuka, K.; Ren, X. Physical metallurgy of Ti-Ni-based shape memory alloys. *Prog. Mater. Sci.* **2005**, *50*, 511–678.
2. Delobelle, V.; Chagnon, G.; Favier, D.; Alonso, T. Study of electropulse heat treatment of cold worked NiTi wire: From uniform to localised tensile behaviour. *J. Mater. Process. Technol.* **2016**, *227*, 244–250.
3. Jiang, S.; Zhao, Y.; Zhang, Y.; Li, H.; Liang, Y. Effect of solution treatment and aging on microstructural evolution and mechanical behavior of NiTi shape memory alloy. *T. Nonferr. Met. Soc.* **2013**, *23*, 3658–3667.
4. Tadayyon, G.; Mazinani, M.; Guo, Y.; Zebarjad, S.M.; Tofail, S.A.; Biggs, M.J. The effect of annealing on the mechanical properties and microstructural evolution of Ti-rich NiTi shape memory alloy. *Mater. Sci. Eng. A* **2016**, *662*, 564–577.
5. Tadayyon, G.; Mazinani, M.; Guo, Y.; Zebarjad, S.M.; Tofail, S.A.; Biggs, M.J. Study of the microstructure evolution of heat treated Ti-rich NiTi shape memory alloy. *Mater. Charact.* **2016**, *112*, 11–19.
6. Kuang, C.-H.; Chien, C.; Wu, S.-K. Multistage martensitic transformation in high temperature aged Ti 48 Ni 52 shape memory alloy. *Intermetallics* **2015**, *67*, 12–18.
7. Wang, X.; Verlinden, B.; Van Humbeeck, J. Effect of post-deformation annealing on the R-phase transformation temperatures in NiTi shape memory alloys. *Intermetallics* **2015**, *62*, 43–49.

8. Zhao, C.; Zhao, S.; Jin, Y.; Meng, X. Nanoscale interwoven structure of B2 and R-phase in Ni-Ti alloy film. *Vacuum* **2016**, *129*, 45–48.
9. Jiang, S.; Zhang, Y.; Zhao, Y.; Liu, S.; Li, H.; Zhao, C.-Z. Influence of $Ni_4Ti_3$ precipitates on phase transformation of NiTi shape memory alloy. *Trans. Nonferr. Met. Soc.* **2015**, *25*, 4063–4071.
10. Resnina, N.; Belyaev, S.; Zeldovich, V.; Pilyugin, V.; Frolova, N.; Glazova, D. Variations in martensitic transformation parameters due to grains evolution during post-deformation heating of Ti-50.2 at.% Ni alloy amorphized by HPT. *Thermochim. Acta* **2016**, *627*, 20–30.
11. Shahmir, H.; Nili-Ahmadabadi, M.; Huang, Y.; Jung, J.M.; Kim, H.S.; Langdon, T.G. Shape memory effect in nanocrystalline NiTi alloy processed by high-pressure torsion. *Mater. Sci. Eng. A* **2015**, *626*, 203–206.
12. Yu, C.; Aoun, B.; Cui, L.; Liu, Y.; Yang, H.; Jiang, X.; Cai, S.; Jiang, D.; Liu, Z.; Brown, D.E. Synchrotron high energy X-ray diffraction study of microstructure evolution of severely cold drawn NiTi wire during annealing. *Acta Mater.* **2016**, *115*, 35–44.
13. Shi, X.; Guo, F.; Zhang, J.; Ding, H.; Cui, L. Grain size effect on stress hysteresis of nanocrystalline NiTi alloys. *J. Alloys Compd.* **2016**, *688*, 62–68.
14. Li, Y.; Li, J.; Liu, M.; Ren, Y.; Chen, F.; Yao, G.; Mei, Q. Evolution of microstructure and property of NiTi alloy induced by cold rolling. *J. Alloys Compd.* **2015**, *653*, 156–161.
15. Ke, C.; Cao, S.; Zhang, X. Phase field modeling of Ni-concentration distribution behavior around $Ni_4Ti_3$ precipitates in NiTi alloys. *Comp. Mater. Sci.* **2015**, *105*, 55–65.
16. Jiang, S.; Hu, L.; Zhang, Y.; Liang, Y. Nanocrystallization and amorphization of NiTi shape memory alloy under severe plastic deformation based on local canning compression. *J. Non-Cryst. Solids* **2013**, *367*, 23–29.
17. Jiang, S.; Ming, T.; Zhao, Y.; Li, H.; Zhang, Y.; Liang, Y. Crystallization of amorphous NiTi shape memory alloy fabricated by severe plastic deformation. *Trans. Nonferr. Met. Soc.* **2014**, *24*, 1758–1765.
18. Bataillard, L.; Bidaux, J.-E.; Gotthardt, R. Interaction between microstructure and multiple-step transformation in binary NiTi alloys using in-situ transmission electron microscopy observations. *Philos. Mag. A* **1998**, *78*, 327–344.
19. Allafi, J.K.; Ren, X.; Eggeler, G. The mechanism of multistage martensitic transformations in aged Ni-rich NiTi shape memory alloys. *Acta Mater.* **2002**, *50*, 793–803.
20. Dlouhý, A.; Bojda, O.; Somsen, C.; Eggeler, G. Conventional and in-situ transmission electron microscopy investigations into multistage martensitic transformations in Ni-rich NiTi shape memory alloys. *Mater. Sci. Eng. A* **2008**, *481*, 409–413.